IEEE Access
Multidisciplinary | Rapid Review | Open Access Journal

Received February 8, 2020, accepted March 12, 2020, date of publication March 24, 2020, date of current version April 13, 2020.

Digital Object Identifier 10.1109/ACCESS.2020.2983090

Research on Transient DC Bias Analysis and Suppression in EPS DAB DC-DC Converter

TIANLI DAI[1,2], (Student Member, IEEE), JINGGANG QIN[1], GAO GE[1], CHAO ZHOU[1,3], LICAN HE[4], JINGYU ZHAI[5], AND JIANGANG LI[1]

[1]Institute Plasma Physics, Chinese Academy of Science, Hefei 230031, China
[2]Science Island Branch, University of Science and Technology of China, Hefei 230031, China
[3]Energy, Material and System Group, TNW, University of Twente, 7500AE Enschede, The Netherlands
[4]Hefei Boao Electric Technology Company, Ltd., Hefei 230002, China
[5]School of Electrical and Automation Engineering, Hefei University of Technology, Hefei 230002, China

Corresponding author: Chao Zhou (chao.zhou@ipp.ac.cn)

This work was supported in part by the Strategic Priority Research Program of Chinese Academy of Sciences under Grant XDB25000000, in part by the Fund of Natural Science Foundation of China under Grant 51677184, in part by the National Key Research and Development Plan under Grant 2019YFC0117502, and in part by the National High Level Research Project.

ABSTRACT During excitation and demagnetization phase for the superconducting magnet, in dual-active-bridge (DAB) converter based power supply, a dc bias may occur in high-frequency transformer and thus lead to the faults. In this paper, an improved transient extend-phase-shift (TEPS) control strategy is proposed to suppress the dc bias without any additional hardware. Unlike the traditional extend-phase-shift (EPS) strategy, the voltages of the transformer are asymmetrical for half a period after changing phase-shift and then remain symmetrical. This makes it take half a switching period for the current of transformer to reach the steady state, and then eliminates the dc bias. The experiment verifies the performance on dc bias suppression. This method provides a good theoretical and experimental basis for the EPS DAB DC-DC converter to realize the optimal control for excitation and demagnetization system in high-field superconducting magnet power supply (SMPS).

INDEX TERMS Dual-active-bridge (DAB), dc bias, transient extend-phase-shift (TEPS) control strategy, high-field SMPS.

I. INTRODUCTION

With the development of life and material science, there is an increasing demand for imagining tools with high magnet field such as high-field Magnetic Resonance Imaging (MRI) and high-field Nuclear Magnetic Resonance (NMR). Superconducting magnet power supply (SMPS) is an important component to excite and demagnetize the superconducting magnet. According to system demands, SMPS requires small volume, high power density, high reliability and isolated bidirectional energy flow [5]. The high-frequency (HF) isolated transformer (TF) instead of the line-frequency transformer should be employed in isolated bidirectional dc/dc converters to provide voltage matching and galvanic isolation, with the advantages of less weight, volume and higher power density. Dual-active-bridge (DAB) converter, which has many advantages of high power density, easily realized soft-switching, bidirectional power transfer capability, modularity and symmetric structure, has gradually attracted more investigations [6], [7].

A power supply based on DAB converter is designed and developed. It includes a PWM rectifier, a DAB converter to realize bidirectional energy flow, and a full-bridge to change voltage polarity, as shown in Figure 1.

Insofar, most of the researches on DAB converter have been focused on the soft-switching solution, phase-shift (PS) control strategy, current stress minimization, dead time compensation, topology extension, hardware design and optimization [8], [9]. However, the dc bias characteristic is less studied. In fact, the dc component of primary and secondary inductance current signal of high frequency transformer is the average value of current signal in a switching cycle. For the suppression of dc component, it can be divided into software and hardware suppression related to the causes. Practically,

The associate editor coordinating the review of this manuscript and approving it for publication was Sing Kiong Nguang.

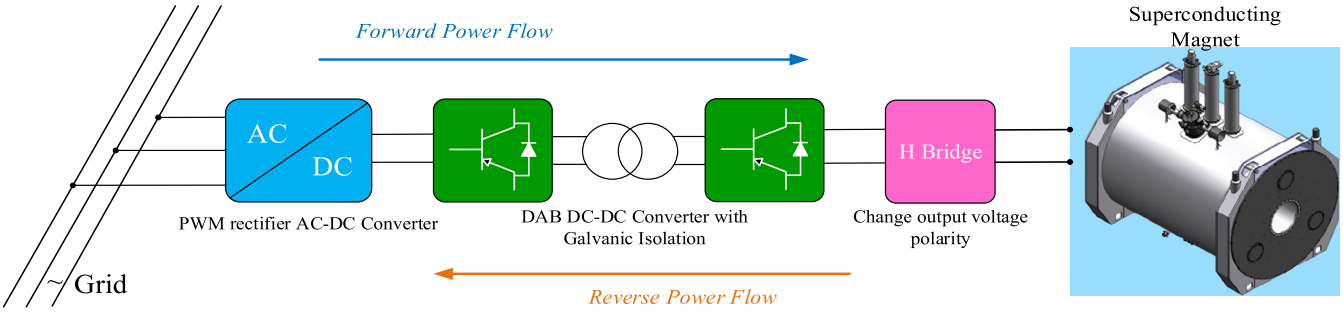

FIGURE 1. Typical topology structure for SMPS.

the factors that may cause dc bias are as follows: 1) the asymmetry of circuit parameters, e.g the delay of driving pulse signal, inconsistency between on-state voltage drop in switches, deferences in on-state switches resistance, etc.; 2)the fluctuation of input and output dc voltage during a period; and 3) the adjustment of the PS ratio derived from the power changing [10].

The existence of dc bias makes the current waveform of DAB DC-DC HF TF asymmetric with high current stress, leading to the magnetization curve of transformer core no longer symmetrical to the origin when it operates. As the magnetization curve is nonlinear, when the magnetization is serious, the iron core enters the single direction deep saturation, resulting in a sharp increase of unidirectional magnetization current, increasing loss, even causing damage to the switch tube. This affects the working reliability of the DAB converter, may cause quench and even permanent damage for the superconducting magnet. Meanwhile, there is a risk of bursting in the sudden increasing of the cold screen pressure, which should be avoid in the excitation and demagnetization [11], [12]. Comparing with factor 1 and 2, the factor 3 is more serious. This is determined by the law of PS in control circuit driving signal and cannot be improved simply by the hardware design optimization.

The transient PS control strategy is adopted to analyze the transient process of load in [10]. Based on the derivation of the expression of dc component current, the recurrence of the PS ratio and dc bias are established and the dc bias can be suppressed by compensating the phase-shift ratio. However, that paper is based on SPS control strategy, which is not suitable for EPS control strategy in practice. In [13], the EPS control strategy is proposed and the operation principle and modes are analyzed. Besides, the control performances of SPS and EPS control are analyzed comparatively by establishing mathematical models of transmission power, backflow power and current stress. However, the paper does not analyze the mechanism and method of restraining DC bias. The virtual direct power control method is used to control the feedforward link of the converter, which improves the dynamic response speed of the DAB converter. Nonetheless, the control strategy of the transient DC component has not been analyzed in [14].

Based on EPS control strategy, a comprehensive theoretical analysis of the transient dc bias and the TEPS control strategy are proposed to eliminate the dc bias. This paper is organized as follows: 1) the power transmission and steady characteristics are analyzed in order to conclude the change mode of inner and outer PS ratio; 2) the transient dc bias is explained with the PS ratio changing; 3) the improvement transient control strategy method is proposed to suppress dc bias; 4) the engineering implementation and dynamic analysis are presented; 5) the comparison test is given to verify the analysis and conclusion.

II. STEADY CHARACTERISTIC and POWER TRANSMISSION

In this analysis, the forward power flow is defined from the Vi side to the Vo side, the reverse power flow is defined from the Vo side to the Vi side. Thus, the leading and lagging voltages in the forward power flows are V_{AB} and V_{CD}. Equally, leading and lagging voltages are V_{CD} and V_{AB} in the reverse power flows. Here, the forward power flow is analyzed by examples, and the reverse power flow similarity omit no analysis.

A. STEADY CHARACTERISTIC

The topology is shown in Fig. 2, L is the sum of the inductance of the leakage inductance of the HF TF and series auxiliary inductance; n is TF turn ratio; $V1$ and $V2$ are dc input and output source voltages; $vh1$ and $vh2$ are on behalf of the full-bridge H_1 and full-bridge H_2; V_{AB} and V_{CD} are the ac output voltages of $vh1$ and $vh2$; i_L is the current of inductance L;

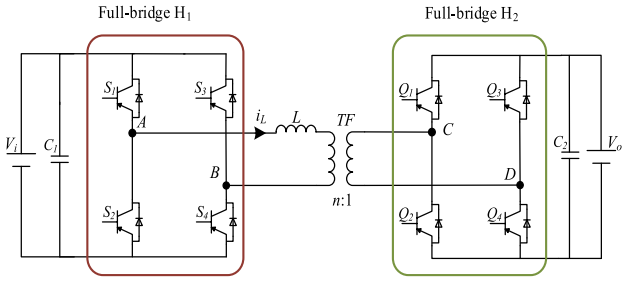

FIGURE 2. The topology structure of DAB DC-DC converter.

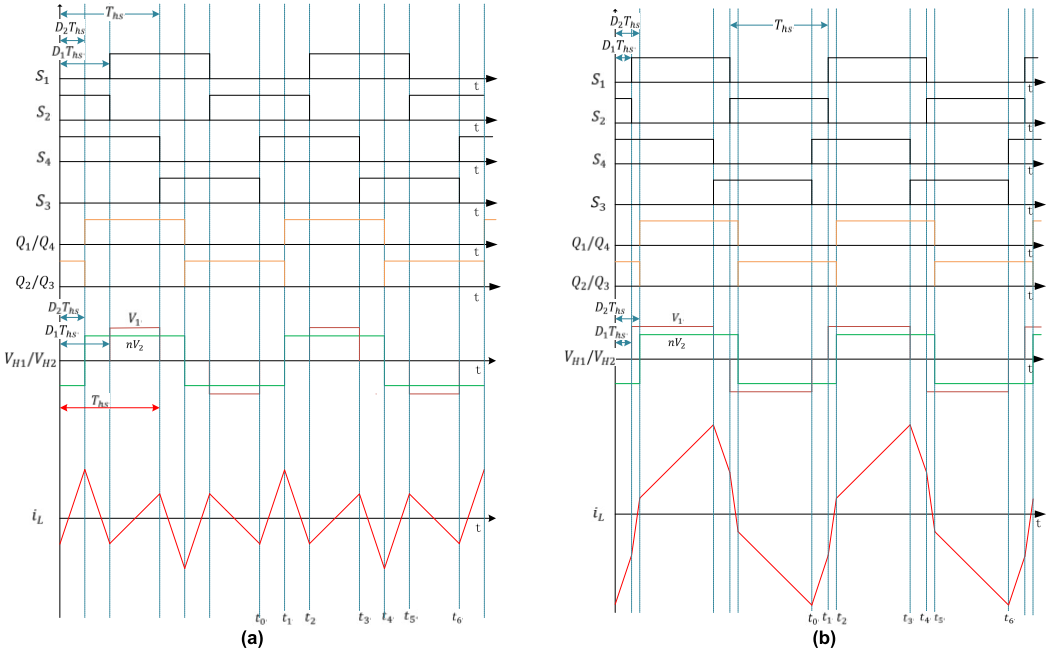

FIGURE 3. The control schematic diagram of EPS DAB. (a) $0 =< D_1 =< D_2 <= 1$. (b) $0 <= 0.5D_1 <= D_2 <= D_1 <= 1$.

T_{hs} is half a switching period, $fs = 1/(2Ths)$ is switching frequency, and D_1 and D_2 are the inner and outer PS ratios in half a switching period; where $k = V1/nV2$ is the voltage conversion ratio. In this section, we just analyze the steady characteristic and power transmission of EPS control strategy in the forward power flow.

In case of forward power flow, there are two situations [13] as shown in Fig. 3. Here, when the control mode of Fig.3a is adopted, that means $0 =< D_1 =< D_2 <= 1$.

It is defined that $i_L(t_0)$ and I_0 is the current of t_0, $i_L(t_1)$ and I_1 is the current of t_1 *et al,* as shown in Fig. 3 and formula 1. And the following definitions of figures and formula are the same.

According to the principle of current i_L positive and negative symmetry, those are listed in formula (2) in half a switching period.

$$\begin{cases} i_L(t_0) = -i_L(t_3) = i_L(t_6) \\ i_L(t_1) = -i_L(t_4) \\ i_L(t_2) = -i_L(t_5) \end{cases} \tag{1}$$

Then, we get

$$\begin{cases} I_0 = -\dfrac{nV_2T_{hs}}{2L}\left[2D_2 - 1 + k(1-D_1)\right] \\ I_1 = -\dfrac{nV_2T_{hs}}{2L}\left[2D_2 - 2D_1 - 1 + k(1-D_1)\right] \\ I_2 = \dfrac{nV_2T_{hs}}{2L}\left[1 + k(2D_2 - D_1 - 1)\right] \\ I_3 = \dfrac{nV_2T_{hs}}{2L}\left[2D_2 - 1 + k\,(1-D_1)\right] \end{cases} \tag{2}$$

B. POWER TRANSMISSION

So the transmission power is:

$$\begin{aligned} P_{EPS} &= \frac{1}{T_{hs}}\int_0^{T_{hs}} V_{AB}i_L(t)dt \\ &= \frac{nV_1V_2}{2f_sL}\left\{\begin{array}{c}(D_2-D_1)\left[1-(D_2-D_1)\right] \\ +\dfrac{1}{2}D_1\left[1-D_1-2(D_2-D_1)\right]\end{array}\right\} \end{aligned} \tag{3}$$

For the convenience of analysis, the unified transmission power P_{EPS} are defined as

$$\begin{aligned} p_{EPS} = \frac{P_{EPS}}{P_N} &= 4(D_2-D_1)[1-(D_2-D_1)] \\ &\quad + 2D_1[1-D_1-2(D_2-D_1)] \end{aligned} \tag{4}$$

where

$$P_N = \frac{nV_1V_2}{8f_sL} \tag{5}$$

Making the outer PS ratio (D_2) minus the inner PS ratio (D_1) and the inner PS D_1 as independent variables in EPS control, then letting the transmission power P_{EPS} be dependent variable, the 3-D curves are shown in figure 4. That concludes EPS control strategy (the constraints are $0 =< D_1 =< D_2 <= 1$) can transmit power in full range. In fact, EPS DAB converter transmits power energy under this constraint. So in this paper, it is just studied with the condition that of $0 =< D_1 =< D_2 <= 1$.

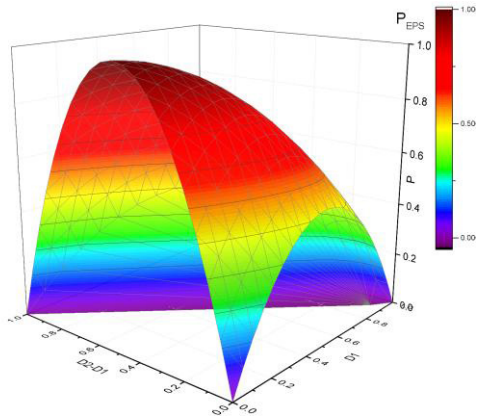

FIGURE 4. Relation 3-D curves of the unified transmission power P_{EPS} with D_1 and D_2.

III. TRANSIENT CHARACTERIZATION OF THE EPS CONTROL STRATEGY

For the superconducting magnet system, after the excitation is completed, the power supply is disconnected, and meanwhile the superconducting magnet operates in a closed-loop with superconducting switches. During demagnetization, the magnet energy is fed back to the power grid through the power supply. So it is necessary to study power changes in single direction, in terms of the following four situations: forward power flow increasing, forward power flow decreasing, reverse power flow increasing and reverse power flow decreasing.

As mentioned above, the forward power flow just need to be studied.

In EPS control strategy, the change of transmission power only needs to change the inner PS ratio D_1 and the outer PS ratio D_2. There are three modes to change the PS: 1) D_1 fixed and D_2 changed; 2) D_2 fixed and D_1 changed; 3) D_1 changed and D_2 changed. All in all, the time-base of S_3 and S_4 in *vh1* lag is fixed. The specific analysis is given bellow.

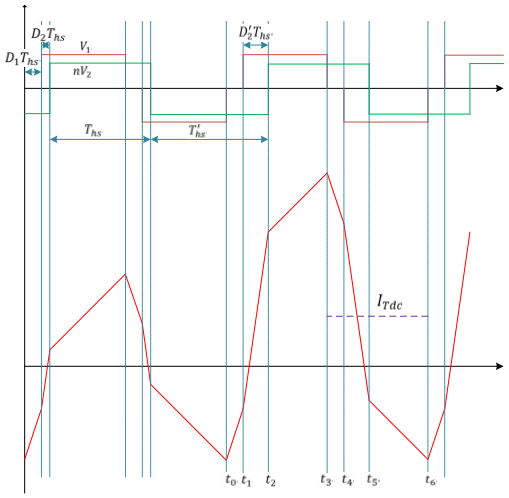

FIGURE 5. Transient waveforms under the EPS control strategy with D_1 fixed and D_2 increasing.

A. D_1 FIXED AND D_2 CHANGED

Here we can let $D_2' > D_2 > 0$. The condition that $D_2 > D_2' > 0$ is analyzed similarly. The transient waveforms of DAB are shown as Fig. 5.

In Fig. 5, the outer PS ratio is D_2 before t_0 and is D_2' after t_0. Thus,

$$T_{hs}' = T_{hs} + D_2'T_{hs} - D_2T_{hs}. \tag{6}$$

Here, the transformer voltages at the primary and secondary sides are still symmetrical after changing outer PS D_2 at t_0. So I_0 equals to I_6, which is not equal to actual I_6 in steady characteristic as shown in Fig. 3a and formula (3). As a consequence, the dc bias I_{Tdc} occurs.

According to Fig. 5, the HFL peak currents can be derived as

$$\begin{cases} I_1 = -\dfrac{nV_2T_{hs}}{2L}\left[2D_2 - 2D_1 - 1 + k(1-D_1)\right] \\ I_2 = \dfrac{nV_2T_{hs}}{2L}\left[2D_2' - 2D_2 + 1 + k(2D_2' - D_1 - 1)\right] \\ I_3 = \dfrac{nV_2T_{hs}}{2L}\left[-2D_2 + 4D_2' - 1 + k(1-D_1)\right] \\ I_4 = \dfrac{nV_2T_{hs}}{2L}\left[4D_2' - 2D_2 - 2D_1 - 1 + k(1-D_1)\right] \\ I_5 = \dfrac{nV_2T_{hs}}{2L}\left[4D_2' - 4D_2 - 1 + k(D_1 - 2D_2 + 1)\right] \\ I_6 = -\dfrac{nV_2T_{hs}}{2L}\left[2D_2 - 1 + k(1\text{-}D_1)\right]. \end{cases} \tag{7}$$

So, the dc bias I_{Tdc} is as follows

$$I_{Tdc} = \frac{I_3 + I_6}{2} = \frac{nV_2T_{hs}}{2L}(2D_2' - 2D_2). \tag{8}$$

According to the formula (8), transient dc bias in this situation is proportional to the increment $(D_2' - D_2)$.

B. D_2 FIXED AND D_1 CHANGED

Here it might be $D_1 > D_1' > 0$. The transient waveforms under the EPS control strategy are shown in Fig. 6. The *vh2* lag is fixed, then the S_1 and S_2 of *vh1* lag PS ratios are changed.

According to Fig. 6, we have

$$\begin{cases} I_1 = -\dfrac{nV_2T_{hs}}{2L}\left[2D_1' - 2D_2 + 1 + k(1-D_1)\right] \\ I_2 = \dfrac{nV_2T_{hs}}{2L}\left[1 + k(2D_2 + D_1 - 2D_1' - 1)\right] \\ I_3 = \dfrac{nV_2T_{hs}}{2L}\left[2D_2 - 1 + k(D_1 - 2D_1' + 1)\right] \\ I_4 = \dfrac{nV_2T_{hs}}{2L}\left[2D_2 - 2D_1' - 1 + k(D_1 - 2D_1' + 1)\right] \\ I_5 = \dfrac{nV_2T_{hs}}{2L}\left[-1 + k(D_1 - 2D_2 + 1)\right] \\ I_6 = -\dfrac{nV_2T_{hs}}{2L}\left[2D_2 - 1 + k(1-D_1)\right]. \end{cases} \tag{9}$$

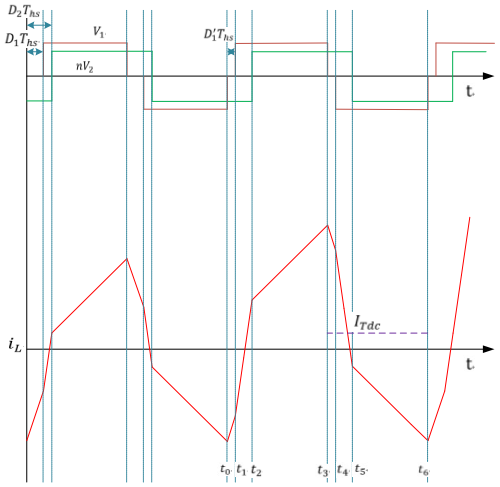

FIGURE 6. Transient waveforms under the EPS control strategy with D_1 decreasing and D_2 fixed.

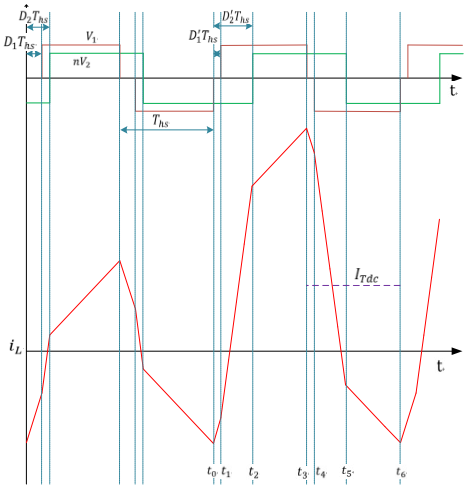

FIGURE 7. Transient waveforms under the EPS control strategy with D_1 decreasing and D_2 increasing.

The dc bias is

$$I_{Tdc} = \frac{I_3 + I_6}{2} = \frac{k \times nV_2T_{hs}}{2L}(D_1 - D_1'). \tag{10}$$

C. D_1 CHANGED AND D_2 CHANGED

Unlike the situation under single PS ratio changing, the phase of the lag *vh*2 is changed with the phase of the S_1 and S_2 changing compared to S_3 and S_4. So the inner PS ratio D_1 and the outer PS ratio D_2 are both changed. In a word, time-base of S_3 and S_4 in *vh1* lag is fixed. Here D_2 increases and D_1 decreases. The transient waveforms are shown in Fig. 7. After t_0, the inner PS ratio and outer PS ratio changes.

According to Fig. 7, the peak current can be get as followed

$$\begin{cases} I_1 = \dfrac{nV_2T_{hs}}{2L}\left[2D_1' - 2D_2 + 1 + k(1 - D_1)\right] \\ I_2 = \dfrac{nV_2T_{hs}}{2L}\left[-2D_2 + 2D_2' + 1 + k(2D_2' + D_1 - 2D_1' - 1)\right] \\ I_3 = \dfrac{nV_2T_{hs}}{2L}\left[-2D_2 + 4D_2' - 1 + k(D_1 - 2D_1' + 1)\right] \\ I_4 = \dfrac{nV_2T_{hs}}{2L}\left[-2D_2 + 4D_2' - 2D_1' - 1 + k(D_1 - 2D_1' + 1)\right] \\ I_5 = \dfrac{nV_2T_{hs}}{2L}\left[-2D_2 + 2D_2' - 1 + k(D_1 - 2D_2' + 1)\right] \\ I_6 = -\dfrac{nV_2T_{hs}}{2L}\left[2D_2 - 1 + k(1\text{-}D_1)\right]. \end{cases} \tag{11}$$

So the dc bias is

$$\begin{aligned} I_{Tdc} &= \frac{I_3 + I_6}{2} = \frac{nV_2T_{hs}}{2L}\left[2D_2' - 2D_2 + k(D_1 - D_1')\right] \\ &= \frac{nV_2T_{hs}}{2L}(2D_2' - 2D_2) + \frac{k \times nV_2T_{hs}}{2L}(D_1 - D_1'). \end{aligned} \tag{12}$$

Due to the formula (8) (10) and (12), the dc bias in this situation is the sum of the first two dc bias. If the polarities of the first two are the same, then the dc bias is larger which may cause greater current stress on transformer. In actual operation, this situation should be well considered.

IV. IMPROVEMENT TRANSIENT CONTROL METHOD

In order to reduce the transient dc bias and the consequent current stress, in this chapter, an improved transient control strategy is put forward and defined as the TEPS method.

A. TEPS IN D_1 FIXED AND D_2 CHANGED

The phase change for the lagging full-bridge *vh*2 is divided into two parts and *vh*1 is fixed as shown in Fig. 8. Before t_0, the outer PS is D_2; the first half a switching period after t_0, the outer PS ratio is D_2''; after that, the outer PS ratio is D_2'. These two parts are added to the rising and falling edges of the lagging voltage in next two T_{hs} after t_0.

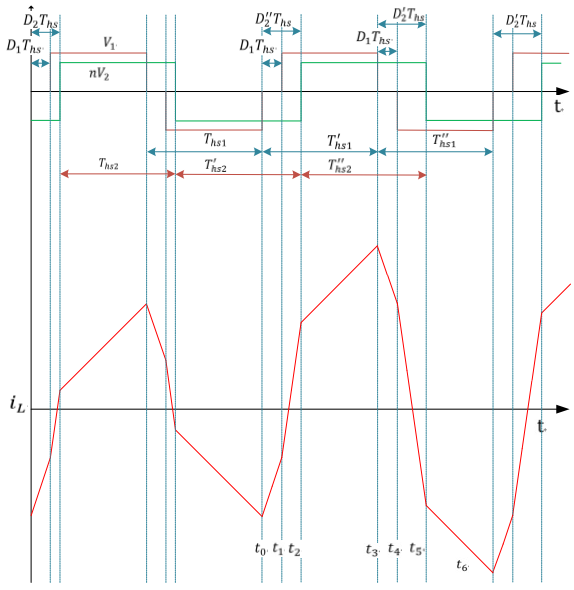

FIGURE 8. Transient waveforms under the TEPS control strategy with D_1 fixed and D_2 increasing.

Here, T_{hs1} is the S_3/S_4 duration of *vh1*, and T_{hs2} is the high-level or low-level duration of *vh2*. The following definitions of T_{hs1} and T_{hs2} are related to this.

Then we have

$$\begin{cases} T''_{hs1} = T'_{hs1} = T_{hs1} \\ T_{hs1} = T_{hs2} = T_{hs} \end{cases}$$
$$\begin{cases} T'_{hs2} = T_{hs2} + (D''_2 - D_2)T_{hs2} \\ T''_{hs2} = T_{hs2} + (D'_2 - D''_2)T_{hs2}. \end{cases} \quad (13)$$

According to formula (13), the peak currents can be derived as

$$\begin{cases} I_1 = \dfrac{nV_2T_{hs}}{2L}\left[2D_1 - 2D_2 + 1 + k(D_1 - 1)\right] \\ I_2 = \dfrac{nV_2T_{hs}}{2L}\left[2D''_2 - 2D_2 + 1 + k(2D'_2 - D_1 - 1)\right] \\ I_3 = \dfrac{nV_2T_{hs}}{2L}\left[4D''_2 - 2\mathrm{D}_2 - 1 + k(1 - D_1)\right] \\ I_4 = \dfrac{nV_2T_{hs}}{2L}\left[4D''_2 - 2D'_2 - 2D_2 - 1 + k(-D_1 + 1)\right] \\ I_5 = \dfrac{nV_2T_{hs}}{2L}\left[4D''_2 - 2D'_2 - 2D_2 - 1 + k(D_1 - 2D'_2 + 1)\right] \\ I_6 = -\dfrac{nV_2T_{hs}}{2L}\left[4D''_2 - 4D'_2 - 2D_2 + 1 + k(1\text{-}\mathrm{D}_1)\right]. \end{cases} \quad (14)$$

And the dc bias I_{Tdc} can be obtained by

$$I_{Tdc} = \frac{I_3 + I_6}{2} = \frac{nV_2T_{hs}}{2L}(4D''_2 - 2D'_2 - 2D_2). \quad (15)$$

Eliminating the dc bias means that I_{Tdc} is zero, then

$$D''_2 = \frac{D_2 + D'_2}{2}. \quad (16)$$

The transformer currents become symmetrical over half switching period under the TEPS control strategy. As a result, the dc bias is eliminated.

B. TEPS IN D_2 FIXED AND D_1 CHANGED

The phase change of the lagging S_1/S_2 for the full-bridge $vh1$ is split into two parts and $vh2$ is fixed. Before t_0, the inner PS is D_1; the outer PS ratio is D''_1 in the first half switching period after t_0; after that, the outer PS ratio is D'_1. As the S_3/S_4 of $vh1$ lag is fixed, then

$$\begin{cases} T''_{hs1} = T'_{hs1} = T_{hs1} \\ T_{hs1} = T_{hs2} = T_{hs}. \end{cases} \quad (17)$$

According to the formula (17) and Fig. 9, the current of transformer is as follows.

Then they can be derived as

$$\begin{cases} I_1 = \dfrac{nV_2T_{hs}}{2L}\left[2D''_1 - 2D_2 + 1 + k(1 - D_1)\right] \\ I_2 = \dfrac{nV_2T_{hs}}{2L}\left[1 + k(2D_2 + D_1 - 2D''_1 - 1)\right] \\ I_3 = \dfrac{nV_2T_{hs}}{2L}\left[2D_2 - 1 + k(D_1 - 2D''_1 + 1)\right] \\ I_4 = \dfrac{nV_2T_{hs}}{2L}\left[2D_2 - 2D'_1 - 1 + k(D_1 - 2D''_1 + 1)\right] \\ I_5 = \dfrac{nV_2T_{hs}}{2L}\left[-1 + k(D_1 + 2D'_1 - 2D_2 - 2D''_1 + 1)\right] \\ I_6 = \dfrac{nV_2T_{hs}}{2L}\left[-2D_2 + 1 + k(\mathrm{D}_1 - 1)\right]. \end{cases} \quad (18)$$

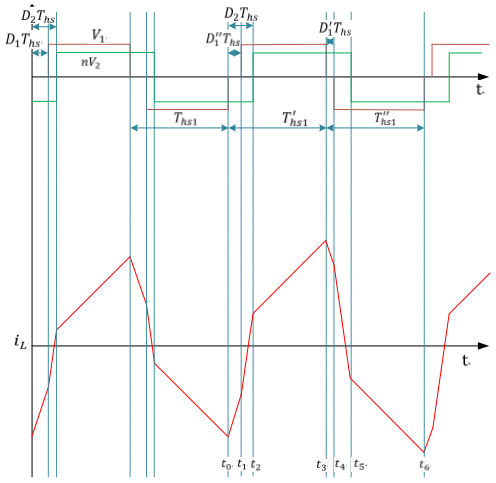

FIGURE 9. Transient waveforms under the TEPS control strategy with D_1 decreasing *and* D_2 fixed.

So the dc bias is

$$I_{Tdc} = \frac{I_3 + I_6}{2} = \frac{nV_2T_{hs}k}{2L}(D_1 + D'_1 - 2D''_1). \quad (19)$$

If I_{Tdc} equals to 0, then

$$D''_1 = \frac{D_1 + D'_1}{2}. \quad (20)$$

Similar to the previous conclusion that TEPS in D_1 fixed and D_2 changed, the transformer currents become symmetrical over one switching period under the TEPS D_2 fixed and D_1 changed using formula (20).

C. TEPS IN D_1 CHANGED AND D_2 CHANGED

The voltage and current waveforms of transformer in TEPS are shown in Fig 10. Based on the previous analysis, in the first half period of changing the PS, the inner and outer PS can

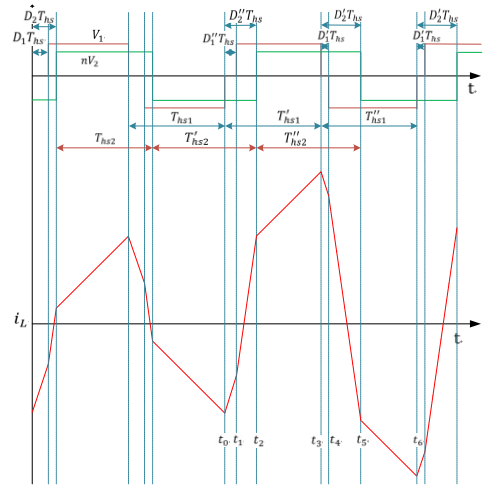

FIGURE 10. Transient waveforms under the TEPS control strategy with D_1 increasing and D_1 decreasing.

be changed to a certain transient value. Before t_0, the outer PS is D_2; the outer PS ratio is D_2'' in the first half switching period after t_0; after that, the outer PS ratio is D_2'. As for the inner PS, the inner PS is D_1 before t_0; the inner PS ratio is D_1'' in the first half switching period after t_0; after that, the inner PS ratio is D_1'. Then, we have

$$\begin{cases} T''_{hs1} = T''_{hs1} = T_{hs1} \\ T'_{hs2} = T_{hs2} + (D''_2 - D_2)T_{hs2} \\ T''_{hs2} = T_{hs2} + (D'_2 - D''_2)T_{hs2} \\ T_{hs1} = T_{hs2}. \end{cases} \tag{21}$$

So the current waveforms of transformer can be listed as

$$\begin{cases} I_1 = \dfrac{nV_2T_{hs}}{2L}\left[2D''_1 - 2D_2 + 1 + k(1 - D_1)\right] \\ I_2 = \dfrac{nV_2T_{hs}}{2L}\left[2D''_2 - 2D_2 + 1 + k(2D''_2 + D_1 - 2D''_1 - 1)\right] \\ I_3 = \dfrac{nV_2T_{hs}}{2L}\left[4D''_2 - 2D_2 - 1 + k(D_1 - 2D''_1 + 1)\right] \\ I_4 = \dfrac{nV_2T_{hs}}{2L}\left[4D''_2 - 2D_2 - 2D'_1 - 1 + k(D_1 - 2D''_1 + 1)\right] \\ I_5 = \dfrac{nV_2T_{hs}}{2L}\left[4D''_2 - 2D_2 - 2D'_2 \right. \\ \qquad \left. -1 + k(D_1 + 2D'_1 - 2D'_2 - 2D''_1 + 1)\right] \\ I_6 = \dfrac{nV_2T_{hs}}{2L}\left[4D''_2 - 2D_2 - 4D'_2 \right. \\ \qquad \left. +1 + k(2\mathrm{D}'_1 + \mathrm{D}_1 - 2\mathrm{D}''_1 - 1)\right]. \end{cases} \tag{22}$$

And I_{Tdc} is obtained as

$$I_{Tdc} = \frac{I_3 + I_6}{2} = \frac{nV_2T_{hs}}{2L}\begin{bmatrix} 4D''_2 - 2D_2 - 2D'_2 \\ +k(D_1 + D'_1 - 2D''_1) \end{bmatrix}. \tag{23}$$

Let I_{Tdc} equal to 0 for any k, then we can get

$$\begin{cases} 4D''_2 - 2D_2 - 2D'_2 = 0 \\ D_1 + D'_1 - 2D''_1 = 0 \end{cases} \tag{24}$$

thus

$$\begin{cases} D''_2 = \dfrac{D_2 + D'_2}{2} \\ D''_1 = \dfrac{D_1 + D'_1}{2}. \end{cases} \tag{25}$$

From formula (21)-(25), transformer currents become symmetrical over a half switching period and the dc bias is eliminated. In addition, compared with formula (16) (20) and (25), it concludes that the TEPS method in the inner and outer PS changing at same time synthesizes only the inner PS changing and only the outer PS changing.

V. MODULATION ALGORITHM AND DYNAMIC RESPONSE

A. TEPS MODULATION ALGORITHM

The proposed TEPS control strategy to decrease the transient dc bias is just enabled during the transient process. By the way, the power transmission characteristic is basically consistent with the traditional EPS control.

In the digital controller modulation algorithm, the time-based counter operates in up-down mode which can generate an asymmetrical the pulse-width-modulation (PWM) waveform. In this mode, the time-based counter starts from zero and increases until the period value N is reached, then the counter decreases until it reaches zero. At this point the counter repeats the pattern and begin to increment. So

$$T_{PWM} = 2 \times N \times T_{TBCLK} = 2T_{hs}. \tag{26}$$

Here, TBCLK is defined as the time-based clock and TPWM is the period of each switching cycle. The time-based counter is synchronized in all PWM pulse modules. The counter-compare submodule containing the counter-compare A (CMPA) and counter-compare B (CMPB) registers and action-qualifier submodule are used to change PS ratios duty cycle. In our subject as shown in Fig. 11, the phase of S_2 PWM equals to the time-based counter. The PS of S_1 PWM comparing with S_4 is the inner PS D_1. For instance, the phase shift of Q_1/Q_4 PWM against S_4 is the outer PS D_2. Furthermore, S_4 and S_2, S_3 and S_4, Q_2/Q_3 and Q_1/Q_4 complement each other with dead zone in case of the same bridge passing through. Here the time-based counter value of N_1 and N_2 can be expressed as

$$\begin{cases} N_1 = [D_1 N] \\ N_2 = [D_2 N]. \end{cases} \tag{27}$$

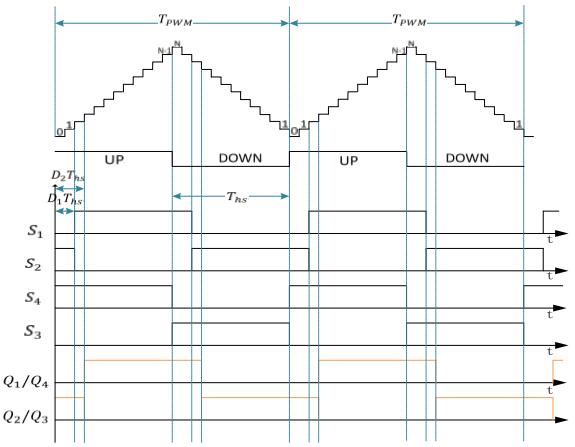

FIGURE 11. The waveforms of digital controller modulation algorithm.

In the formula (27), [x] is the Integral Function, that is the largest integer less or equal to x. It can be seen that the larger N is, the more accurate of the PS controlling is. Then when the period of each switching cycle T_{PWM} is fixed, the larger N means the smaller T_{TBCLK} which correlates positively with T_{cpu}, where T_{cpu} is the reciprocal of the microcontroller operating frequency f_{cpu}.

The integer variable Cnt is used as the timed-based discrete counter, where $0 \leq Cnt < 2N$. In order to adopt the TEPS control strategy during the transient process, the digital controller will detect and store the PS ratios in real time,

TABLE 1. Teps modulation algorithm.

Power flow	Transient status	S_4=1, S_3=0	S_1=1, S_2=0	Q_1/Q_4=1, Q_2/Q_3=0
Forward power flow	D_1 to D'_1, D_2 fixed	$0 \le Cnt < N$	$(N_1+N'_1)/2 \le Cnt < N'_1+N$	$N_2/2 \le Cnt < N/_2+N$
	D_2 to D'_2, D_1 fixed	$0 \le Cnt < N$	$N_1/2 \le Cnt < N_1+N$	$(N_2+N'_2) \le Cnt < N'_2+N$
	D_1 to D'_1, D_2 to D'_2	$0 \le Cnt < N$	$(N_1+N'_1) \le Cnt < N'_1+N$	$(N_2+N'_2) \le Cnt < N'_2+N$

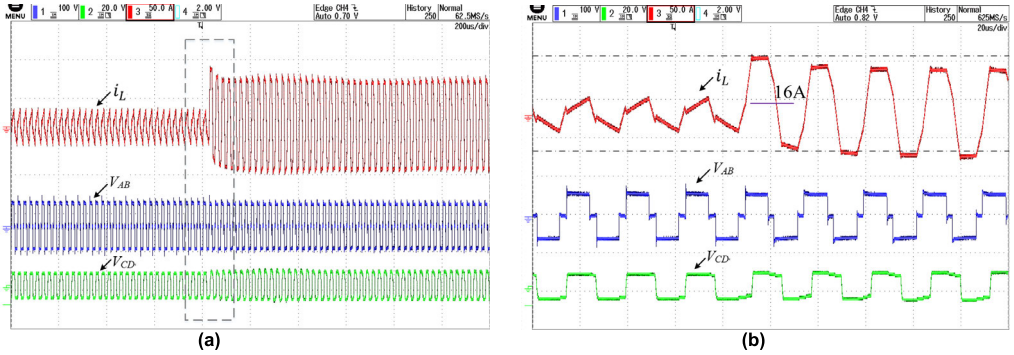

FIGURE 12. The transient waveform in EPS strategy with D_2 changed and D_1 fixed.

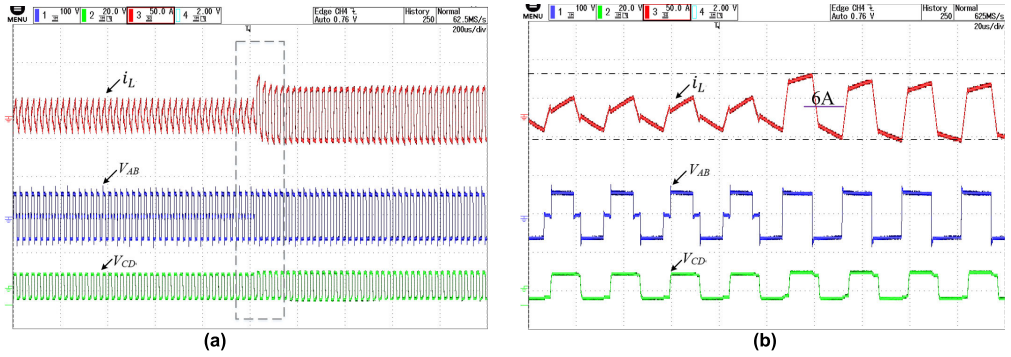

FIGURE 13. The transient waveform in EPS strategy with D_1 changed and D_2 fixed.

then the corresponding PWM waveforms will be updated as shown in Table 1.

B. DYNAMIC RESPONSE

The HF isolated transformer current in the transient process can be divided into ac and dc components shown below:

$$i_L(t) = i_{Tac} + i_{Tdc}. \tag{28}$$

where i_{Tac} is the ac component of steady state and $i_{T\mathrm{dc}}$ is the dc component generated by the transient dc bias.

To some extent, the dynamic response time means the attenuation velocity of the dc bias. It needs to be noted that this paper mainly discusses the performance caused by the EPS and TEPS control strategies and the response time caused by open-loop control parameters. In DAB converter, due to the existence of auxiliary inductance L and the resistance R, the dc component i_{Tac} will decay exponentially with time. The circuit mathematical model can be listed as follows

$$i_{Tdc} = I_{Tdc} e^{-\frac{t}{\tau}} = I_{Tdc} e^{-\frac{R}{L}t} \tag{29}$$

where $\tau = L/R$ is the decay time constant, and $I_{T\mathrm{dc}}$ is the maximum value of the dc component determined by the transient dc bias.

In the traditional EPS control strategy, the dynamic response is determined by circuit parameters, which may be slow in certain condition. However, with TEPS control strategy, the transformer currents become symmetrical over half a switching period. Therefore, the dynamic response will be improved. Theoretically, the dynamic response time is only half of the switching period in TEPS DAB dc-dc converter.

VI. EPPERIMENTAL VERIFICATION

A. EXPERIMENTAL CONDITIONS

In order to verify the theoretical analysis proposed in this paper, a DAB prototype has been constructed. Both the input and output sides of the DAB converter are connected by voltage power supply source. The main parameters are as follows: $V_1 = 60V$, $V_2 = 6V$, $L = 28.5\ \mu H$, $C_1 = C_2 = 13$ mF, $n = 8$ and $fs = 40$ kHz. The dead-time

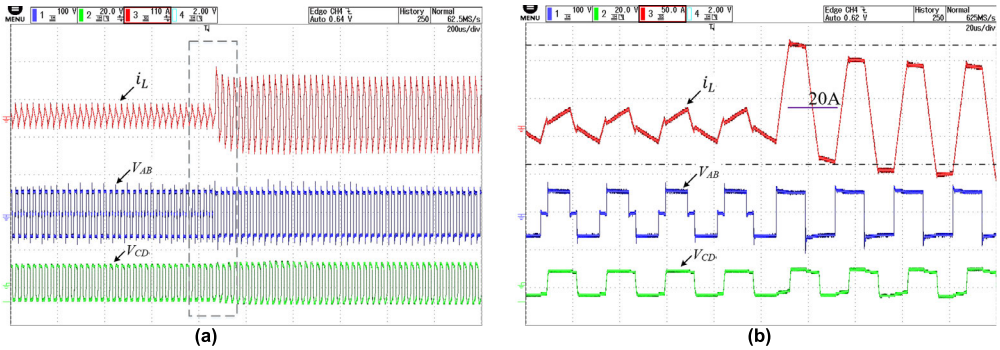

FIGURE 14. The transient waveform in EPS strategy with D_1 decreased and D_2 increased.

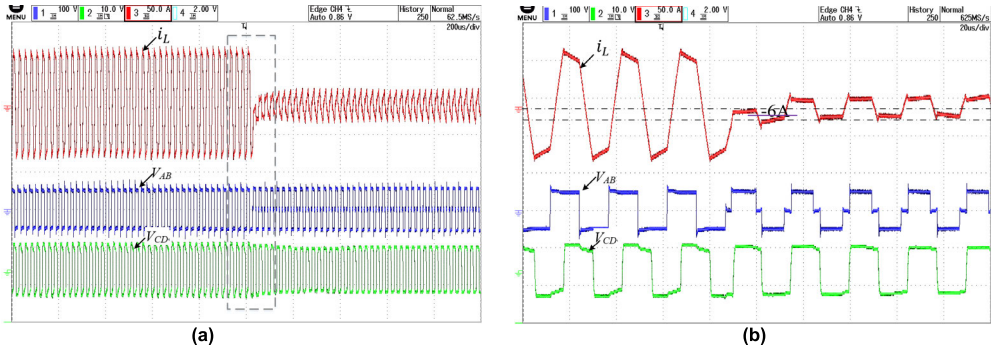

FIGURE 15. The transient waveform in EPS strategy with D_1 increased and D_2 decreased.

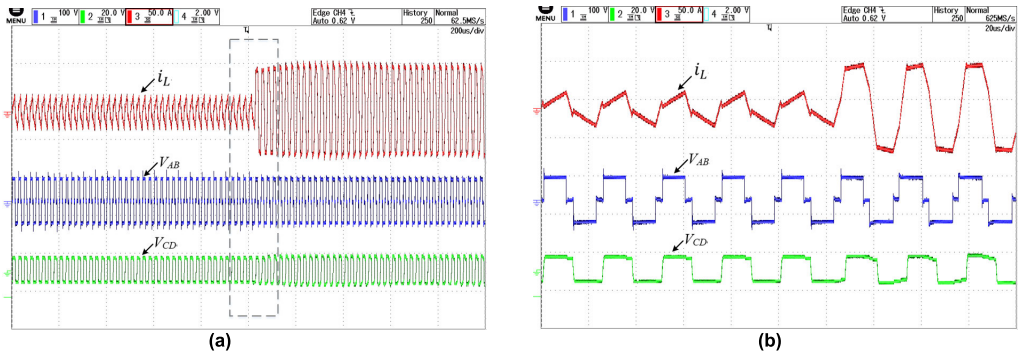

FIGURE 16. The transient waveform in TEPS strategy with D_2 changed and D_1 fixed.

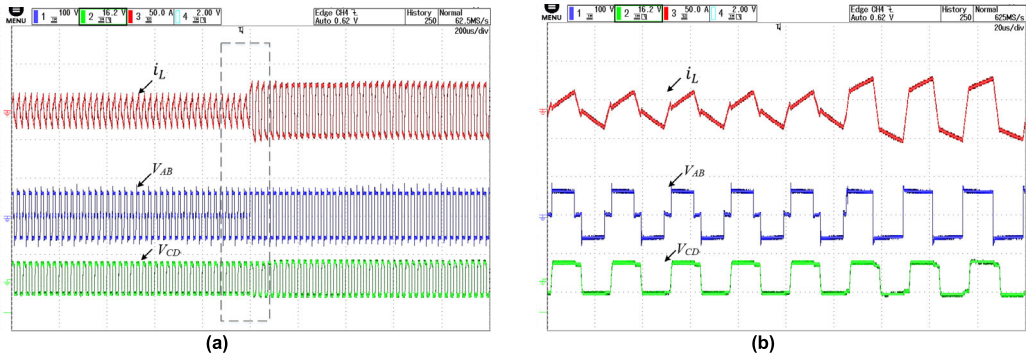

FIGURE 17. The transient waveform in TEPS strategy with D_1 changed and D_2 fixed.

of PWM equals to 0.5 μs. Here, the currents are measured by a high-precision ac/dc current probe TCP 303A and an amplifier TCPA 300, the voltages are measured with a 200 MHz differential probe DP 6150B, and all the waveforms are connected to a 200 MHz/2.5 GS/s oscilloscope DLM3024.

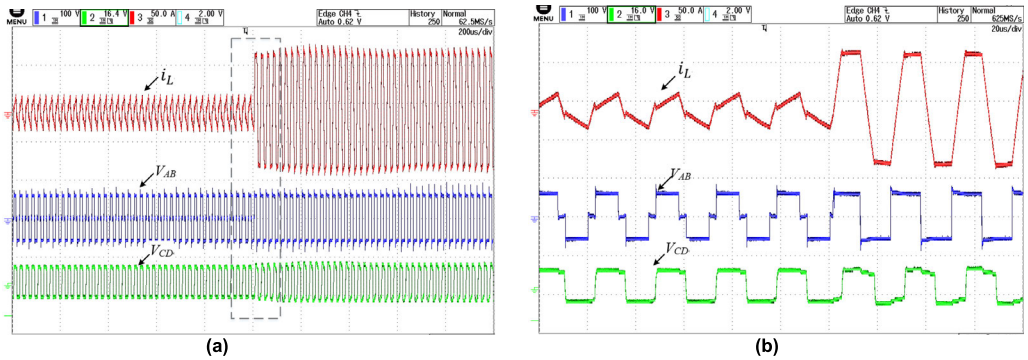

FIGURE 18. The transient waveform in TEPS strategy with D_1 decreased and D_2 increased.

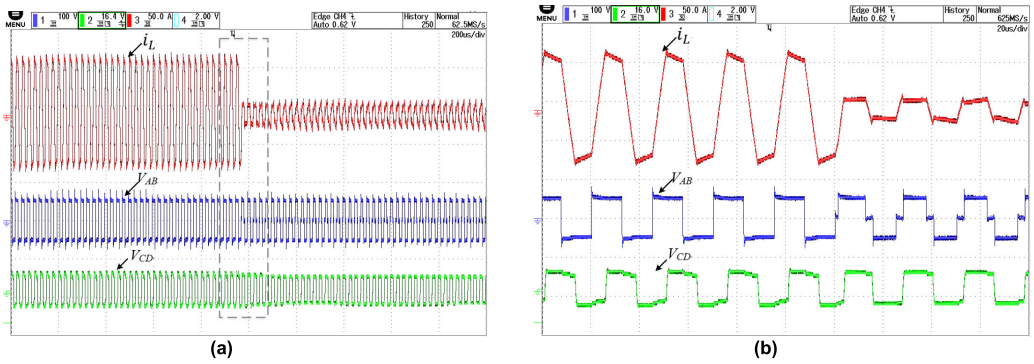

FIGURE 19. The transient waveform in TEPS strategy with D_1 increased and D_2 decreased.

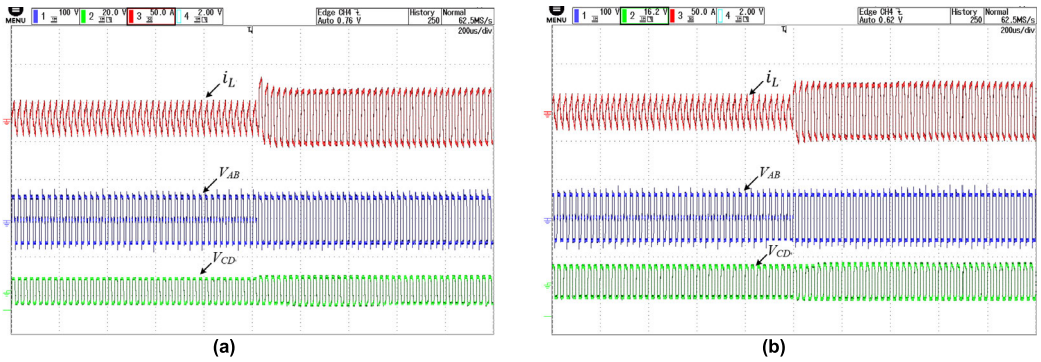

FIGURE 20. The comparison of dynamic response between EPS and TEPS strategies. (a)EPS. (b)TEPS.

B. TRANSIENT EXPERIMENTS IN EPS STRATEGY

Fig. 12-15 shows the transient experimental waveforms in the EPS control strategy, where (b) is the dotted box enlarged view of (a) in all figures. In Fig. 12, the outer PS D_2 increases from 0.2 to 0.45 with the inner PS $D_1 = 0.2$ fixed. In Fig. 13, the inner PS D_1 decreases from 0.2 to 0 with the outer PS $D_2 = 0.2$ fixed. In Fig. 14, the outer PS D_2 increases from 0.2 to 0.45 with inner PS D_1 decreasing from 0.2 to 0. It is obvious that there are different degrees of positive dc bias. And the larger the power change, the more obvious the dc bias is. Those above are the cases of the power up, Fig. 15 shows the case of the power dips with the outer PS D_2 decreasing from 0.45 to 0.2 with the inner PS D_1 increasing from 0 to 0.2. And the negative dc bias appears.

C. TRANSIENT EXPERIMENTS UNDER TEPS STRATEGY

The parameter changes in the all of situations under TEPS strategy are the same as those under the EPS strategy; Fig. 16-19 shows the transient experimental waveforms under the TEPS control strategy. It can be seen clearly that currents become symmetrical and the transient dc biases are eliminated. Furthermore, the current stress is smaller than those under EPS control strategy in all cases.

D. DYNAMIC RESPONSE

The analysis of dynamic performances is to compare the dynamic response of the TEPS and EPS control strategies under the same parameters. A certain situation with inner PS D_1 decreasing and outer PS D_2 fixed is listed in Fig. 20 and other situations are similarly to be omitted. In Fig. 20, the experimental parameters and waveforms coincide with that in Fig. 13 and Fig. 17. The dynamic response time in TEPS is only half of the switching period, which is consistent with previous theoretical analysis. And it can be clearly seen that the dynamic response is slower under the EPS strategy.

VII. CONCLUSION

In this paper, the transient dc bias in EPS DAB converter has been theoretically analyzed and verified by experiments. In transient operation, as the HF isolated TF i_{Tdc} is not steady current when changing the PS ratio due to symmetrical voltages, a dc bias may occur with traditional EPS control strategy, and could lead to faults. The dc bias is closely related with the adjustment of the PS ratio derived from the power change. An improved TEPS control strategy is proposed to optimize the PS ratio in the second half period and then suppress the dc bias. As a result, the safe operation of the converter is compromised. This study explains the phenomenon of dc bias of full power flow in EPS control strategy mode, and recommends effective methods to improve transient performance for SMPS.

REFERENCES

[1] T. F. Budinger, M. D. Bird, L. Frydman, J. R. Long, T. H. Mareci, W. D. Rooney, B. Rosen, J. F. Schenck, V. D. Schepkin, A. D. Sherry, D. K. Sodickson, C. S. Springer, K. R. Thulborn, K. Uğurbil, and L. L. Wald, "Toward 20 T magnetic resonance for human brain studies: Opportunities for discovery and neuroscience rationale," *Magn. Reson. Mater. Phys., Biol. Med.*, vol. 29, no. 3, pp. 617–639, Jun. 2016.

[2] D. L. Bihan and T. Schild, "Human brain MRI at 500 MHz, scientific perspectives and technological challenges," *Supercon. Sci. Thchnol.*, vol. 30, Jan. 2017, Art. no. 033003.

[3] Y. Lvovsky, E. W. Stautner, and T. Zhang, "Novel technologies and configurations of superconducting magnets for MRI," *Superconductor Sci. Technol.*, vol. 26, no. 9, Sep. 2013, Art. no. 093001.

[4] S. Awaji, K. Watanabe, H. Oguro, H. Miyazaki, S. Hanai, T. Tosaka, and S. Ioka, "First performance test of a 25 T cryogen-free superconducting magnet," *Superconductor Sci. Technol.*, vol. 30, no. 6, Jun. 2017, Art. no. 065001.

[5] A. Sinanna, P. M. Aguiar, F. d'Amico, S. Bermond, P. Bredy, A. Donati, C. Hugon, H. Lannou, D. Sakellariou, T. Schild, and P. Tixador, "Field stabilization of the Iseult/Inumac magnet operating in driven mode," *IEEE Trans. Appl. Supercond.*, vol. 20, no. 3, pp. 790–793, Jun. 2010.

[6] Y. Xie, J. Sun, and J. S. Freudenberg, "Power flow characterization of a bidirectional galvanically isolated high-power DC/DC converter over a wide operating range," *IEEE Trans. Power Electron.*, vol. 25, no. 1, pp. 54–66, Jan. 2010.

[7] B. Zhao, Q. Song, W. Liu, and Y. Sun, "Overview of dual-active-bridge isolated bidirectional DC–DC converter for high-frequency-link power-conversion system," *IEEE Trans. Power Electron.*, vol. 29, no. 8, pp. 4091–4106, Aug. 2014.

[8] B. Zhao, Q. Song, W. Liu, and Y. Sun, "Dead-time effect of the high-frequency isolated bidirectional full-bridge DC–DC converter: Comprehensive theoretical analysis and experimental verification," *IEEE Trans. Power Electron.*, vol. 29, no. 4, pp. 1667–1680, Apr. 2014.

[9] D. Costinett, R. Zane, and D. Maksimovic, "Automatic voltage and dead time control for efficiency optimization in a dual active bridge converter," in *Proc. 27th Annu. IEEE Appl. Power Electron. Conf. Expo. (APEC)*, Feb. 2012, pp. 1104–1111.

[10] B. Zhao, Q. Song, W. Liu, and Y. Zhao, "Transient DC bias and current impact effects of high-frequency-isolated bidirectional DC–DC converter in practice," *IEEE Trans. Power Electron.*, vol. 31, no. 4, pp. 3203–3216, Apr. 2016.

[11] A. Sinanna, J. Belorgey, P. Bredy, A. Donati, O. Dubois, Q. Guihard, H. Lannou, A. Lotode, P. Guiho, R. Touzery, and T. Schild, "High reliability and availability of the Iseult/Inumac MRI magnet facility," *IEEE Trans. Appl. Supercond.*, vol. 26, no. 3, pp. 1–5, Apr. 2016.

[12] *Functional Safety of Electrical/Electronic/Programmable Electronic Safety-Related Systems*, Standard NF EN 61508, 2011. [Online]. Available: https://www.afnor.org

[13] B. Zhao, Q. Yu, and W. Sun, "Extended-phase-shift control of isolated bidirectional DC–DC converter for power distribution in microgrid," *IEEE Trans. Power Electron.*, vol. 27, no. 11, pp. 4667–4680, Nov. 2012.

[14] W. Song, N. Hou, and M. Wu, "Virtual direct power control scheme of dual active bridge DC–DC converters for fast dynamic response," *IEEE Trans. Power Electron.*, vol. 33, no. 2, pp. 1750–1759, Feb. 2018.

TIANLI DAI (Student Member, IEEE) was born in Anhui, China, in 1992. He received the bachelor's degree in nuclear engineering and technology from Harbin Engineering University, in 2014. He is currently pursuing the Ph.D. degree in nuclear science and technology with the University of Science and Technology of China, Hefei, China. His current research interests include superconductor magnet power supply topology and control systems.

JINGGANG QIN was born in Shandong, China, in 1980. He received the Ph.D. degree in nuclear engineering and technology from the University of Chinese Academy of Sciences, in 2013. He is currently a Group Leader of superconducting conductor with the Applied Superconductivity Research Laboratory, Institute Plasma Physics, Chinese Academy of Sciences, Hefei. His current research interests include Nb3Sn CICC and Bi2212 high-temperature superconducting magnet.

GAO GE was born in Anhui, China, in 1975. She received the Ph.D. degree in nuclear engineering and technology from the University of Chinese Academy of Sciences, in 2006. She is currently the Group Leader of superconducting magnet power supply with the Power Supply and Control Research Laboratory, Institute Plasma Physics, Chinese Academy of Sciences, Hefei. Her current research interest includes high-power superconducting magnet power supply.

CHAO ZHOU was born in Shandong, China, in 1984. He received the Ph.D. degree in applied superconductivity from the University of Twente, The Netherlands, in 2014. He is currently a Researcher with the Applied Superconductivity Research Laboratory, Institute Plasma Physics, Chinese Academy of Sciences, Hefei. His current research interests include high-field superconducting magnet and YBCO high-temperature superconducting magnet.

LICAN HE was born in Guangxi, China, in 1986. He received the B.Tech. and M.Tech. degrees in electrical engineering from the Hefei University of Technology (HFUT), in 2010 and 2013, respectively. He is currently working in Hefei Boao Electric Technology Co., Ltd. His research interests include step-up power electronics converters (dc/ac and dc/dc), and multilevel inverter topologies and their control.

JINGYU ZHAI was born in Anhui, China, in 1997. He received the bachelor degree in electrical engineering and automation from the Hefei University of Technology, in 2018. He is currently pursuing the master's degree with the energy storage system Laboratory, Hefei University of Technology. His research interests include LLC converter and dual-active-bridge (DAB) dc-dc converter.

JIANGANG LI was born in Anhui, China, in 1961. He received the Ph.D. degree in physics from the University of Chinese Academy of Sciences. He is the Researcher of the Institute of Plasma, a Convener of the National Committee of experts on magnetically confined fusion energy, and the Director of ITER Council. His current research interest includes engineering design of magnetic nuclear fusion.